Extended Abstracts of the 22nd (1990 International) Conference on Solid State Devices and Materials, Sendai, 1990, pp. 1163-1164

LN-D-7

Low Temperature Ion Implantation for Buried Layer Formation

T. SUZUKI, H. YAMAGUCHI, S. OHZONO, and N. NATSUAKI
Device Development Center, Hitachi, Ltd., Ome-shi, Tokyo, 198 Japan

Ion Implantation is an attractive technique to form buried doped-layers for semiconductor device fabrication. However, relatively high dose implantation at room temperature (RT) has not been applied to practical use since it induces high density of residual defects and some of them extend toward the substrate surface. The extended defect generation arises from an unamorphized and heavily damaged region formed in case of light ion implantation such as B implant, or from a diffused boundary between amorphized and crystal regions in case of heavy ion implantation. The diffused amorphous/crystal (a/c) boundary is often formed by spontaneous annealing during implantation. In this paper, it is shown that extremely low temperature implantation offers a promissing approach to remarkably reduce the residual defect density and localize the defects by suppressing point defect migration and thereby amorphization enhancement as well as avoidance of during-implant annealing, even for B implantation.

The CZ (100) Si wafers were implanted with B and P ions at 200keV to doses of 1E14 to 1E15 /cm^2. Substrate temperatures during implantation were varied from RT to -200℃. The implanted samples were then annealed at 900℃ for 30min in dry N_2. As-implanted damages and residual defects were observed using cross-sectional and plan-view TEM. In-situ ellipsometry was employed to monitor damages at implantation temperature and their annealing behaviour during warming the implanted substrates up to RT. Oxygen interaction with residual defects was measured by SIMS as oxygen redistribution profiles.

The implant temperature effects on the features of the damages in as-implanted samples and the residual defects in annealed samples are shown in Figs. 1 and 2 for B 1E15 /cm^2 implantation. In the case of -50℃ or higher temperature implantation, amorphization does not occur and high-density dislocations are observed around the projected range with some dislocations extended along (111) planes. On the other hand, -150℃ or lower temperature implantation results in amorphization and generation of two separated residual defect bands which consist of localized dislocations. The depth of the deeper band corresponds to the original bottom a/c interface and the defects are the so called end-of-range defects. The upper band is located approximately at the center of the buried amorphous layer and therefore considered to be formed by the encounter of the bidirectional solid phase epitaxial recrystallization. It must be noted here that in case of -200℃ implantation, the density of the residual defects is very low, most of dislocations in the upper band lie on a (100) plane and no extented dislocation is ovserved.

The reason for the dramatic temperature dependence mentioned avobe can be attributed to the different during-implant annealing features of point defects in the damage accumulation. Figure 3 shows the extinction coefficient changes measured by the in-situ ellipsometry as a function of temperatures from implant temperature to RT for P 1E14 /cm^2 implantation. The extinction coefficient decreases drastically around -100℃ at which neutral monovacancies are annealed out to form more complex defects. This means during-implant annealing is effectively suppressed below -100℃. In addition, SIMS measurement of oxygen depth profiles after annealing at 900℃ says that sharp oxygen pile-up occurs at the upper defect band in the -200℃ implanted sample as is shown in Fig. 4. This high concentration of oxygen atoms may play a role of effective dislocation pinning. Thus, low temperature implantation is effective to control the residual defect formation.

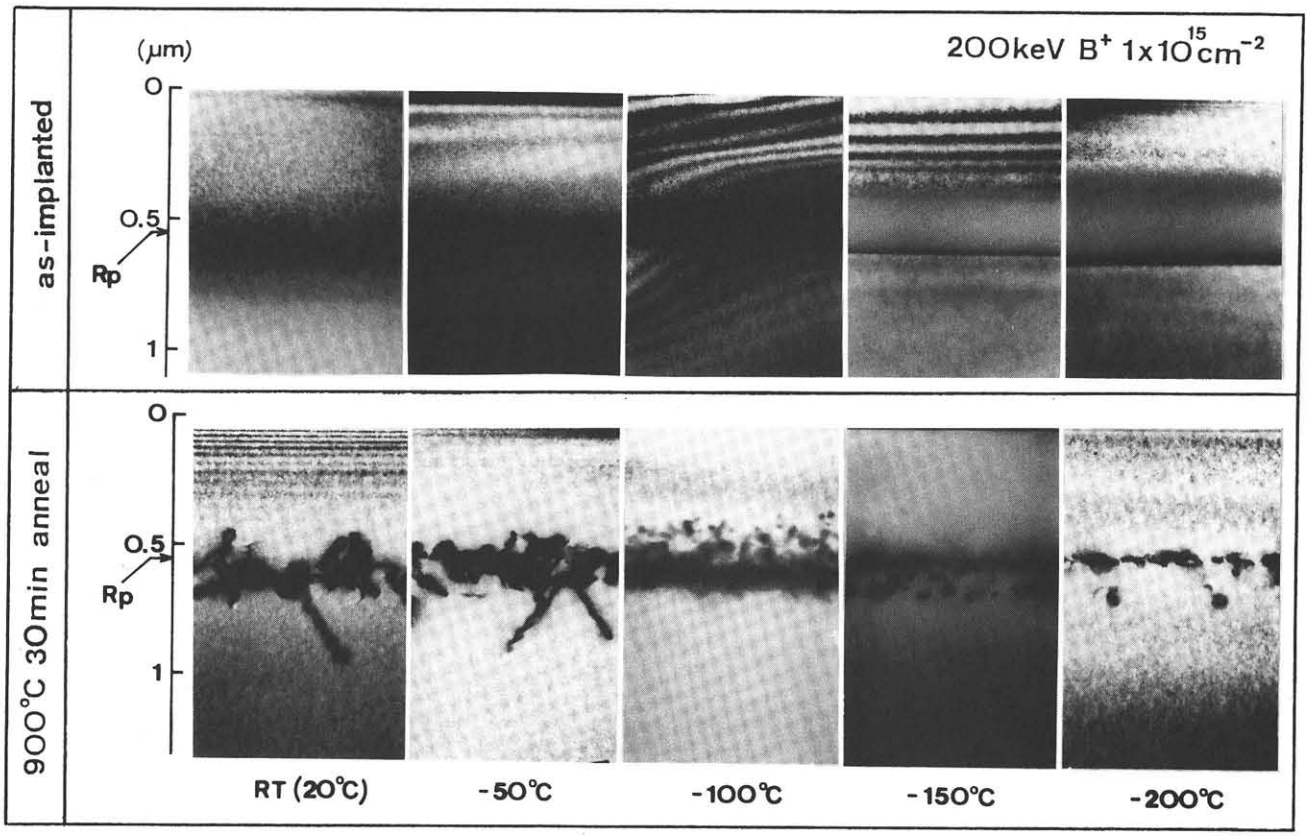

Fig.1 Cross-sectional TEM micrographs showing as-implanted damages and residual defects after annealing.

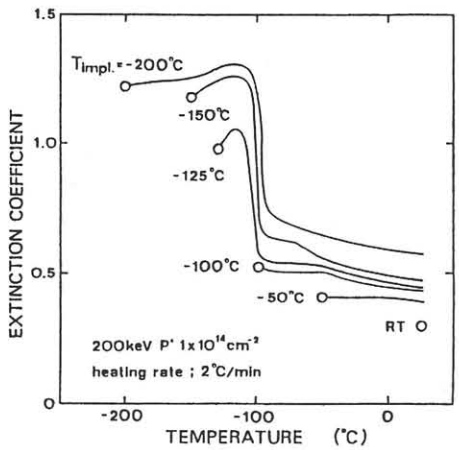

Fig.3 Extinction coefficient as a function of temperature by in-situ ellipsometry.

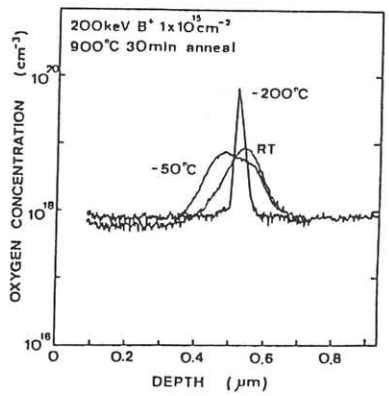

Fig.4 Depth profiles of oxygen atoms after annealing.

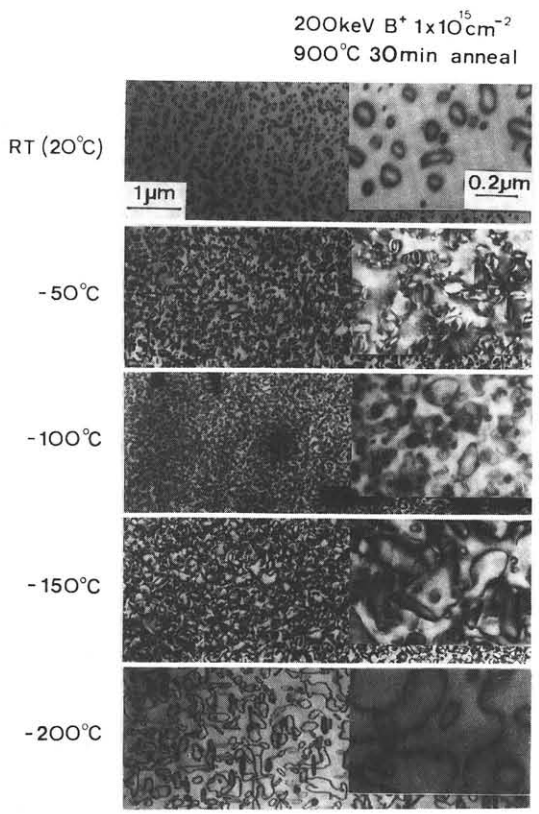

Fig.2 Plan-view TEM micrographs showing residual defects after annealing.